THE JOURNAL OF
PHYSICAL CHEMISTRY
LETTERS
A JOURNAL OF THE AMERICAN CHEMICAL SOCIETY

pubs.acs.org/JPCL Letter

Supercooled Liquid Water Diffusivity at Temperatures near the Glass Transition Temperature

R. Scott Smith,* Wyatt A. Thornley, Greg A. Kimmel, and Bruce D. Kay*

Cite This: *J. Phys. Chem. Lett.* 2025, 16, 3198−3205 Read Online

ABSTRACT: Isotopically layered amorphous solid water films were used to measure the diffusivity of deeply supercooled liquid water near the glass transition. The films, composed of separate $H_2{}^{18}O$ and $H_2{}^{16}O$ layers, were grown by vapor deposition at low temperature and then heated to observe the intermixing of the isotopic layers. Very slow heating rates (as low as 10^{-4} K/s) were used to decouple the diffusion and crystallization processes to ensure that the observed intermixing occurred at temperatures that were well-separated from the onset of crystallization. Numerical simulations of the desorption spectra were used to extract the translational diffusivities. The diffusivities obtained in this paper are consistent with translational liquid-like motion at temperatures near and above the proposed T_g of 136 K. These findings support the idea that the melt of amorphous water, above its glass transition temperature is thermodynamically continuous with normal supercooled liquid.

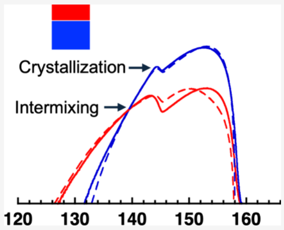

Among water's numerous unusual properties is the unresolved question of whether the behavior of amorphous water above its apparent glass transition at ∼136 K is that of a true supercooled liquid.[1−4] The answer is important for determining if there is thermodynamic continuity between the melt of amorphous water and normal liquid water.[5−9] The glass transition, which is a kinetic transition not a thermodynamic phase transition, is typically defined to occur when molecules are moving too slowly to sample the available configurational space on a laboratory time scale (∼100 s). At the glass transition temperature, T_g, the supercooled liquid's structure is effectively "frozen" as an amorphous solid. When an amorphous solid is heated above its T_g the previously inaccessible configurational degrees of freedom become accessible and the rotational and translational properties of the supercooled liquid reemerge.[10−12]

The formation of amorphous water, as for most liquids, requires cooling rates that are fast enough to circumvent crystallization.[1,11,13,14] For water, this can be accomplished by vapor deposition onto a low temperature ($\lesssim$120 K) substrate.[9,13,15,16] Calorimetric characterizations of amorphous water films report an increase in the heat capacity of ∼2 J/K·mol near 136 K which was interpreted as being due to the glass transition.[17−20] This change in heat capacity is relatively small compared to the change at the melting point where the heat capacity increases by ∼38 J/K·mol. In fact, the increase in the heat capacity from crystalline ice to liquid water is about a factor of 2. Some have argued that the reported glass transition is too weak to be from the unfreezing of translational and orientational (rotational) degrees of freedom expected at the glass transition and that these results may be due to reorientation transitions only.[2,21,22]

Beyond changes in thermodynamic properties, the transformation to a supercooled liquid at the glass transition should also result in the onset of molecular translational motion. Fisher and Devlin conducted infrared experiments to observe isotopic exchange in amorphous water films at ∼125 K and concluded that the molecular motion that develops at the glass transition temperature is due to orientational (rotational) diffusion.[23] Similarly, Shepard and Salzman conducted calorimetric and X-ray diffraction experiments and also concluded that their results support molecular reorientation and not translational motion at the proposed T_g.[24]

In prior work, we used isotopically layered water films to determine the diffusivity of the melt of amorphous water above its T_g and prior to crystallization.[15,25,26] The time evolution of the intermixing was determined by monitoring desorption kinetics from of the outer layer of the film. We found that when heated above its T_g, the intermixing of the isotopic layers was consistent with long-range molecular translation characteristic of liquid-like behavior. However, later work showed that crystallization, which occurred in concert with the intermixing, strongly influenced the results such that they were not representative of translational diffusion in the liquid.[27,28]

In this letter, we revisit the intermixing of isotopically layered amorphous water films using low temperatures and extremely slow heating rates to decouple the diffusion and crystallization processes. This allows us to measure and analyze the intermixing of the amorphous layers without the interference of crystallization. We find liquid like translational

Received: January 24, 2025
Revised: March 18, 2025
Accepted: March 18, 2025
Published: March 20, 2025

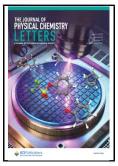

https://doi.org/10.1021/acs.jpclett.5c00245

diffusion near the glass transition. The diffusivity has an Arrhenius temperature dependence with an activation energy of ∼36 kJ/mol.

Evidence for liquid-like translational diffusion in amorphous water films at or near 136 K is displayed in Figure 1. Shown are the temperature-programmed desorption (TPD) spectra for three amorphous water films composed of 20 layers of $H_2{}^{18}O$ deposited on top of 20 layers of $H_2{}^{16}O$ at 90 K. Amorphous water formed by vapor deposition on a cold substrate is referred to as amorphous solid water (ASW).[13,16] After deposition, the composite films were heated to and held at 136 K for various wait times (0, 3600, and 10800 s). After the specific wait time, the films were cooled below 70 K and then heated at a linear rate of 0.5 K/s until desorbed. The bottom set of curves is for the 0 s wait time at 136 K experiment. Initially, desorption is observed only from the top layer ($H_2{}^{18}O$, blue curve) until about 154 K where the onset of desorption from the bottom layer ($H_2{}^{16}O$, red curve) becomes apparent. At ∼159 K there is a decrease in the desorption rates from both layers that results in an apparent "bump" in the TPD spectra. This "bump" is the result of the transformation from the initially higher free energy (higher vapor pressure) amorphous solid to the lower free energy (lower vapor pressure) crystalline phase.[9,16,29] The "bump" in the desorption spectrum is a signature of the crystallization of the ASW film.

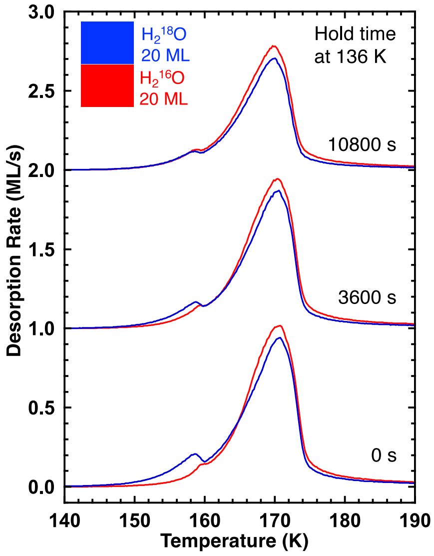

Figure 1. Experimental TPD spectra for amorphous water films composed of 20 layers of $H_2{}^{18}O$ (blue curve) deposited on top of 20 layers of $H_2{}^{16}O$ (red curve) at 90 K. After deposition, the composite films were heated to and held at 136 K for wait times of 0 s (bottom), 3600 s (middle), and 10800 s (top). After the specific wait time, the films were cooled below 70 K and then heated at a linear rate of 0.5 K/s until desorbed.

The middle set of curves in Figure 1 is for the experiment with a wait time of 3600 s. These curves are similar to those for the 0 s wait time experiment except that the onset of desorption from the bottom layer ($H_2{}^{16}O$, red curve) begins at a lower temperature of about 150 K. The top set of curves is for the experiment with a wait time of 10800 s. In this case, the spectra show that the desorption curves for the two isotopes are nearly the same at 140 K which indicates that the two isotopic layers have completely intermixed by this temperature. In contrast, for films annealed at 125 K, where the diffusion rate is considerably smaller, the TPD spectra for films annealed 0 and 10800 s are essentially identical (see SI Figure SI-1).

The experiments show that the intermixing of the isotopic layers increases with wait time and thus provides evidence for translation motion at 136 K. If there was no translational motion, we would expect that the sets of TPD spectra for all the experiments to have the same behavior, independent of the wait time.

It is important to note that the use of nanoscale films and long wait times are requisite to observe translational motion at the extremely low diffusivities (10^{-20}−10^{-22} m^2/s) at temperatures near and just above T_g.

While the results in Figure 1 provide clear, albeit qualitative, evidence for translational diffusion at 136 K, extracting quantitative diffusivities from these types of "wait and flash" experiments can be complicated. One complication is that, while diffusion occurs at 136 K during the isothermal wait time, it also occurs during the heating ramp. Extracting quantitative information requires decoupling the two sources of diffusion. Another complication is that even at low temperatures, there is desorption from the top layer of the composite film. For example, at 136 K the estimated desorption rate for amorphous water is $\sim 1.2 \times 10^{-3}$ ML/s.[30] This means that there can be significant desorption for the longer wait time experiments. For example, for a wait time of 10800 s, at 136 K there should be the loss of ∼13 ML from the film. This is consistent with the experimental results in Figure 1 and is another factor to consider when trying to quantify the diffusivity.

In our prior work using isotopic ASW layers, the observed intermixing occurred at temperatures (150−155 K) in concert with the crystallization of the film.[15,25,26] In those experiments the films were heated at 0.6 K/s. This required us to model the diffusivity as a linear combination of the amorphous and crystalline diffusion weighted by their respective mole fractions. The close coupling of diffusion and crystallization means that extracting the true translational liquid diffusion from intermixing measurements is complicated. Others have shown that additional mechanisms can arise such as mixing through and along cracks that form when ASW crystallizes.[31−34] Here, to simplify the analysis and to eliminate potential specious diffusion mechanisms we conducted experiments using very slow heating rates to decouple the diffusion and crystallization kinetics. Decoupling the diffusion and crystallization kinetics requires that the activation energies for diffusion and crystallization are different. If that is the case, it should be possible to observe intermixing at temperatures that are below, and well-separated from crystallization.

The effect of slowing the heating rate on the intermixing is displayed in Figure 2. Plotted are the results for three experiments for ASW films composed of 20 layers of $H_2{}^{16}O$ deposited on top of 80 layers of $H_2{}^{18}O$ grown at 90 K and then heated with a linear ramp rate. The displayed spectra were obtained with a heating rate of 0.01 K/s (bottom set), of 0.001 K/s (middle set), and of 0.0001 K/s (top set). As expected, the desorption curves shift to lower temperatures with decreasing heating rate. This is due to the activated kinetic processes (desorption, crystallization, and diffusion) having more time to progress at lower temperatures. Note that the use of slow heating rates comes at the cost of a decrease in signal intensity. The spectra show that there is about a 10-fold decrease in signal intensity for every factor of 10 decrease in heating rate. However, even for the slowest heating rate of 0.0001 K/s the

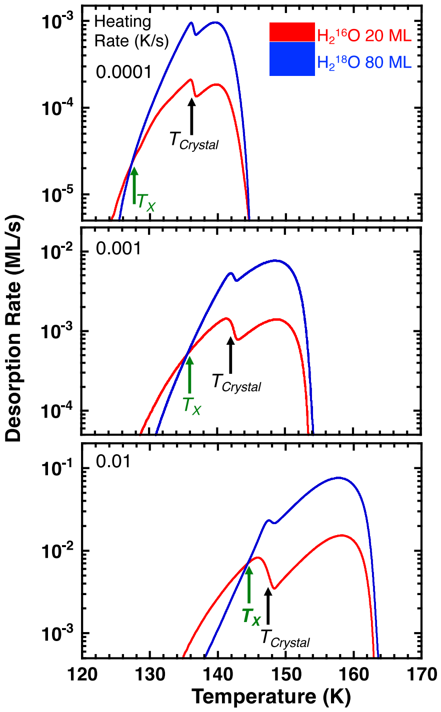

Figure 2. Experimental TPD spectra for amorphous water films composed of 20 layers of $H_2{}^{16}O$ (red line) deposited on top of 80 layers of $H_2{}^{18}O$ (blue line) at 90 K. After deposition, the composite films were heated at rates of 0.01 K/s (bottom set), 0.001 K/s (middle set) and 0.0001 K/s (top set) until completely desorbed. The vertical arrows indicate the crossover, T_x (green arrows), and crystallization, $T_{Crystal}$ (black arrows), temperatures.

signal-to-noise is still very good. This is due to the use of molecular beam deposition, line of sight mass spectrometer detection, and increased signal averaging times. For all heating rates, signals were averaged to give a temperature resolution greater than 0.01 K.

The purpose of using very slow heating rates is to decouple the diffusion and crystallization kinetics. The results in Figure 2 show that as the heating rate decreases, the mixing of the films occurs at lower temperatures relative to crystallization. To demonstrate this point, we can use readily identifiable features in the TPD spectra that are characteristic of intermixing and crystallization to track how they vary with the heating rate. For crystallization, it is convenient to use the decrease in desorption that occurs upon crystallization (Figure 2, vertical black arrows). For intermixing, we use the temperature where the desorption rate from $H_2{}^{16}O$ and $H_2{}^{18}O$ are equal (Figure 2, vertical green arrows) which we will refer to as the "crossover" temperature. For all the heating rate experiments in Figure 2 the crossover temperature is well-separated from the onset of crystallization ("the bump"). However, due to differences between the activation energies for diffusion and crystallization, the temperature shifts are not the same for the two processes. For example, for the 0.01 K/s experiment the temperature difference between the crossover temperature and the crystallization bump is ∼3 K whereas for the 0.0001 K/s experiment the difference is ∼9 K. The reason is that the slower ramp rate experiment spends more time at lower temperatures which allows for the lower activation energy diffusion process to proceed relatively faster than the higher activation energy crystallization process. The effect is similar to that observed in Figure 1. Note that in these experiments the initial film is comprised of 20 layers of $H_2{}^{16}O$ on top of 80 layers of $H_2{}^{18}O$ so that there will always be a crossover temperature where the isotopes have intermixed over a distance of roughly 40 layers.

Figure 3 shows a plot of the diffusive mixing (crossover, solid green circles) and crystallization (solid black circles) temperatures for the experiments in Figure 2 along with the data from two additional heating rate experiments (0.03 and 0.003 K/s). The plot shows that for heating rates below ∼0.2 K/s diffusive intermixing occurs at a lower temperature than crystallization. For heating rates greater than ∼0.2 K/s the reverse is true, that is, crystallization occurs at a lower temperature than diffusive intermixing. The difference between the diffusive intermixing and crystallization temperatures increases with decreasing heating rates. This is a result of the activation energy for diffusion being less than that for crystallization as supported by the slopes of the diffusion (green line) and crystallization (black line) curves in Figure 3. Clearly, using slow heating rates will allow us to measure the translational liquid diffusivity without interference from ASW crystallization.

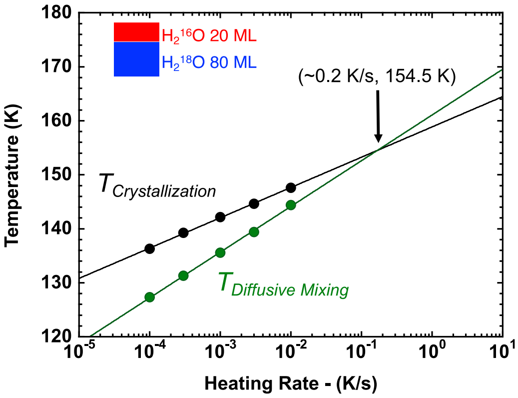

Figure 3. Plot of the diffusive mixing (solid green circles) and crystallization (solid black circles) temperatures versus heating rate for the slow heating rate experiments using amorphous water films composed of 20 layers of $H_2{}^{16}O$ deposited on top of 80 layers of $H_2{}^{18}O$. The heating rates used were 0.01, 0.003, 0.001, 0.0003, and 0.0001 K/s. The diffusive mixing crossover temperature is defined as the temperature where the desorption rates of the two isotopes are equal. The crystallization temperature is defined as when the film is 50% crystallized which is determined by analysis of the "bump" region of the TPD spectrum.

Figure 4 displays the experimental results (solid lines) for the 0.0003, 0.001, and 0.003 K/s experiments (all heating rate experiments are shown in the SI). Analysis of the experimental results was conducted using numerical simulations with a one-dimensional kinetic model where the system was divided into N discrete layers corresponding to the number of layers of the ASW films. We assumed the initial layer concentrations to be 100% $H_2{}^{16}O$ in the top 20 ML and 100% of the $H_2{}^{18}O$ isotope in the bottom 80 ML. Diffusion between the adjacent layers (the layer above and below), was governed by the isotopic concentration gradient between layers and the temperature-dependent diffusivity. Molecules in the top layer were allowed to desorb with a rate dependent on the isotopic mole fraction, the desorption kinetic parameters, and the phase of the film (amorphous or crystalline). The crystallization kinetics were modeled using a differential form of the Avrami equation.[15,29]

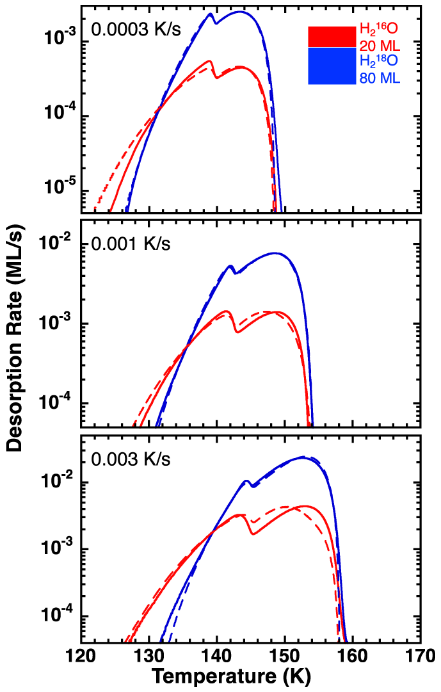

Figure 4. Experimental TPD spectra for amorphous water films composed of 20 layers of $H_2{}^{16}O$ (solid red lines) deposited on top of 80 layers of $H_2{}^{18}O$ (solid blue lines) at 20 K. After deposition, the composite films were heated at rates of 0.003 K/s (bottom set), 0.001 K/s (middle set), and 0.0003 K/s (top set) until completely desorbed. The dashed lines are the corresponding simulation results obtained with diffusion Arrhenius parameters of E_A = 36.82 kJ/mol and prefactors of $\nu = 1.5 \times 10^{-6}$, 1.4×10^{-6}, and 1.2×10^{-6} m^2/s for the 0.003, 0.001, and the 0.0003 K/s simulations, respectively.

The total desorption rate is the sum of the amorphous and crystalline desorption rates weighted by their respective mole fractions. The diffusivity was also weighted by the crystalline mole fraction however the diffusivity for the crystalline phase was set to zero which froze in the isotope distribution when the film had completely crystallized. An Arrhenius temperature dependence, rate = $\nu \exp(-E_A/RT)$, where ν is the prefactor and E_A is the activation energy, was used in the simulations for all kinetic processes. While one would expect these processes to have slightly different rates because of the mass differences, a simple kinetic isotope effect would predict an effect of $(20/18)^{1/2}$ which is about 5%. This is consistent with vapor pressure measurements where a difference of less than 2% is reported,[35] and viscosity measurements where a difference of about 5% is observed.[36] We have also measured the desorption and crystallization kinetics of pure $H_2{}^{16}O$ and $H_2{}^{18}O$ amorphous films and find that the kinetics of the two isotopes are nearly the same (see SI Figure SI-2). Given the relatively small effect, in the simulations we used the same kinetic parameters for the amorphous desorption, crystalline desorption, crystallization kinetics, and the diffusivity for both water isotopes. A more detailed description of the simulation model and the full list of simulation parameters is given in the SI. Note that the diffusivities we report below were extracted from desorption data prior to crystallization.

The results for a set of simulations using the same diffusion activation energy are displayed in Figure 4 as dashed lines. The simulations are in good agreement with the experimental results and quantitatively capture the desorption, crystallization, and diffusion kinetics. An activation energy for diffusion of E_A = 36.82 kJ/mol was used for all the heating rate experiments displayed in Figure 4. The diffusion prefactors varied slightly with $\nu = 1.5 \times 10^{-6}$, 1.4×10^{-6}, and 1.2×10^{-6} m^2/s used for the 0.003, 0.001, and the 0.0003 K/s simulations respectively in Figure 4. However, due to compensation effects, equally reasonable simulation results can be obtained with a range of diffusion activation energy and prefactor combinations. A series of simulations were conducted using a range of diffusion activation energies. The optimal diffusion activation energy was determined by the value that gave the smallest average standard deviation for the set of prefactors needed to simulate the five heating rate experiments. The optimal diffusion activation energy was determined to be $E_A = 36 \pm 4$ kJ/mol and the corresponding diffusion prefactors to be $\nu = 10^{-6.17 \pm 1.58}$ m^2/s. (See SI for more details.)

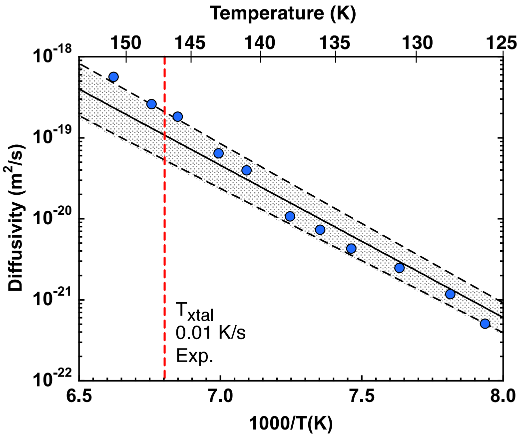

Figure 5. Arrhenius plot of the estimated temperature dependent diffusivity obtained in the current paper (solid black line) (E_A = 35.98 kJ/mol and $\nu = 6.6 \times 10^{-7}$ m^2/s) and our estimated uncertainties (dashed black lines). The diffusivities obtained using the measured crystalline ice growth rates and the Wilson Frenkel model (solid blue circles) in ref 37. The red vertical dashed line at ~147 K is the crystallization temperature for the 0.01 K/s experiment which demarks the highest temperature where our diffusivity measurements were decoupled from crystallization.

Figure 5 displays an Arrhenius plot of the temperature dependent diffusivity obtained in the current paper (solid black line) and our estimated uncertainties (dashed black lines). The vertical dashed line at ~147 K is the crystallization temperature for the 0.01 K/s experiment. Above this temperature crystallization impacts the mixing kinetics.[27,28] We have previously estimated the diffusivity in ASW films using the crystalline growth rate.[37] In those experiments an ASW layer was deposited on top of a crystalline ice layer and then heated to, and held isothermally at, a temperature between 126 and 151 K. In this configuration the crystalline ice layer acts as a nucleation template and the crystallization of the ASW layer is entirely due to a linear growth front.[37−39] The crystalline growth rate of a material can be related to the liquid mobility of molecules at the liquid−solid interface using the Wilson-Frenkel model.[40−44] While the Wilson-Frenkel model does not provide a direct measurement of diffusivity, it is based on reasonable physical arguments and its application often works well.[43,45] The diffusivities obtained from the crystalline ice growth rates and the Wilson-Frenkel model are shown in Figure 5 as solid blue circles.[37] There is good agreement between the diffusivities obtained with the intermixing of isotopic layers (present work) and those extracted using the crystalline ice growth rates. Notice that above ~145 K those diffusivities begin to be higher than our diffusion estimate (solid black line). This is the temperature above which the diffusion activation energy was observed to increase, indicating a strong (Arrhenius) to fragile (super-Arrhenius) transition.[37] Our measured diffusivities are limited to the low temperature, strong temperature dependence regime below 145 K.

In previous work we used the permeation of an inert gas through an amorphous overlayer to measure the diffusivity of various supercooled liquids prior to crystallization.[46−50] In that work we developed universal scaling relationships between the diffusivity, overlayer thickness, and the temperature ramp rate. Using these scaling relationships, we derived simple equations from which the diffusivity can be extracted using the inert gas peak desorption temperature, heating rate, and layer thickness without the need for numerical simulation.[49] Those same scaling relationships and equations were employed using the crossover temperature as a characteristic reference to extract the supercooled liquid diffusivity for the TPD experiments here. The results from the scaling analysis are in good agreement with the simulation results in Figure 5 and are shown in the SI (Figure SI-14).

The experimental diffusivities in this paper demonstrate translational liquid-like motion at temperatures near and above the proposed T_g of 136 K. Our results are in contrast to the interpretations of Fisher and Devlin[23] where they claim that there is no evidence for translation motion and the observed isotope exchange in their experiments was only due to rotations. It is unclear if the experiments of Fisher and Devlin[23] are only sensitive to rotations and not translations as claimed. Similarly, Shephard and Salzmann[24] based their conclusions on calorimetric measurements of ice VI and amorphous ices composed of three water isotopes $H_2{}^{16}O$, $H_2{}^{18}O$, and D_2O. In ice VI the change in the heat capacity at the glass transition is only due to molecular reorientations and not translational motion. They argue that because the isotopic behavior of the amorphous solids was the same as that of ice VI, the changes in the heat capacity at their glass transitions are also only due to molecular reorientations. While these observations are interesting and important, they are not a direct measurement of translation motion, and it is not clear that they can be used to exclude translational diffusion. Note that this has been discussed previously in an excellent review by Amann-Winkel et al.[4] Our experiments were specifically designed to probe only translational motion. It is easy to envision water molecules exhibiting rotation without translation, but it is difficult to imagine how they can translate without rotating due to the strongly anisotropic nature of hydrogen bonds in condensed phases. One possibility is that rotations are faster than translations. Resolving this will require additional research beyond the scope of this paper.

For the results presented here, the coverages were 100 ML or less, which corresponds to film thicknesses of ~33 nm or less. For this thickness range, one concern is that the measured diffusion coefficient might not be representative of bulk water. For example, previous research has shown that enhanced mobility of molecules near a vacuum interface can lead to the formation of exceptionally stable ("ultrastable") glasses.[51] The length scale over which the properties converge to the bulk can, in some cases, be tens of nanometers.[52,53] However, for nanoscale water films, the available data suggests that many properties converge to the bulk within ~2 nm of an interface (e.g., air, vacuum, or solid). For example, the excess free energy and entropy of nanoscale amorphous solid water films at ~130−150 K can be connected to the properties of bulk water at ambient temperatures.[9,29] At higher temperatures, molecular dynamics simulations and experiments indicate density oscillations at liquid water/solid interface that persist for a few layers into the liquid.[54−56] Simulations also indicate that self-diffusion is enhanced perhaps up to 4× in first ~0.3 nm near an water/vacuum interface, but it decreases to within ~20% of the bulk value within 1 nm.[57,58] In contrast, experiments indicate diffusion in nanoscale pores is modestly reduced with respect to bulk water.[59−62] Overall, the existing literature suggests that the self-diffusion is only significantly different in the immediate vicinity of the interface.

Our results also support the interpretation that the relatively small increase in the heat capacity of ~2 J/K·mol near 136 K as being due to the glass transition.[17−20] Arguments against this interpretation are based on the fact that the small change in the heat capacity reported for amorphous water is only ~2% of that observed for water solutions.[2,63] For most systems there is a relatively large abrupt increase the heat capacity at the glass transition temperature as previously "frozen" degrees of freedom (rotations, translations) become accessible. This expectation assumes that the structures of the amorphous solid and supercooled liquid are very different. However, more recent work has shown that the structure of supercooled liquid water is composed of a mixture of low- and high-temperature structural motifs.[64−66] The low-temperature motif is more "ice-like" with a high level of local tetrahedral configurations whereas the high-temperature motif is akin to the normal liquid above the melting temperature. The composition of supercooled liquid water varies smoothly with temperature with the low temperature structure being dominant below 135 K and the high-temperature structure being dominant above 245 K. This may explain why near T_g the transition from the highly coordinated amorphous solid to a supercooled liquid whose structure also includes a high degree of coordination does not result in a large increase in the heat capacity.

The experimental results on the intermixing of isotopically layered nanoscale ASW films presented here provide strong evidence for translational liquid-like water diffusion at temperatures near 136 K. The observations required very slow heating rates to allow for sufficient time at low temperatures to observe diffusion and to decouple the diffusion and crystallization kinetics. The diffusivities were obtained over a temperature range from 125 to 145 K and are consistent with those obtained using the crystal ice growth rate and the Wilson-Frenkel model. These findings support the idea that the melt of amorphous water above its glass transition temperature is thermodynamically continuous with normal supercooled liquid water near the melting point.

■ EXPERIMENTAL METHODS

The experiments were performed in an ultrahigh vacuum UHV chamber (base pressure <1.0×10^{-10} Torr) that has been described before in detail.[67] Briefly, the ASW films were created by deposition from a quasi-effusive molecular beam onto a graphene covered 1 cm diameter Pt(111) sample at normal incidence at a temperature of 70 K. Amorphous water films deposited using a well-collimated molecular beam at normal and near normal deposition angles have been shown to be relatively dense and smooth.[68,69] Therefore, we do not think that surface roughness is a factor in the intermixing of the isotopic layers. Furthermore, there is no evidence of dewetting or other morphological changes until the water films crystallize.[70,71] The molecular beam just overfills the sample which helps to minimize the background signal and increase the detection sensitivity. The sample was spot-welded to two tantalum wire leads clamped in a Cu jig attached to a closed cycle He cryostat and resistively heated through the Ta leads. The temperature was monitored with a K-type thermocouple spot-welded to the back of the sample and controlled by computer. Temperature was calibrated using the amorphous water desorption rates calculated from the published vapor pressure data.[30] The error in the absolute temperature was estimated to be less than ±2 K. The TPD spectra of the deposited films were obtained with a quadrupole mass spectrometer in a line-of-sight configuration about 1 cm from the sample. The line-of-sight configuration increases the signal intensity by about a factor of 10 compared to background desorption detection methods.

■ ASSOCIATED CONTENT

Supporting Information

The Supporting Information is available free of charge at https://pubs.acs.org/doi/10.1021/acs.jpclett.5c00245.

> Plot of the wait time experiments conducted at 125 K, plot comparing the desorption and crystallization kinetics of pure $H_2{}^{16}O$ and $H_2{}^{18}O$ amorphous films, plots of the temperature-programmed desorption (TPD) and simulation (for $E_A = 36.82$ kJ/mol) results for all five heating rate experiments displayed on linear–linear and semilog plots, more detail about the simulation model along with the desorption and crystallization kinetic parameters used in the simulations, diffusion prefactors (ν) and activation energies (E_A) that accurately predict the crossover temperature for the mixing of the isotopic layers, analysis of these parameters to estimate the optimal set of diffusion parameters, a comparison of the supercooled liquid water diffusivity obtained from numerical simulations described in the main manuscript with those obtained using equations derived from scaling relationships, and the parameters used for calculating the diffusivities in Figure SI-14 (PDF)

■ AUTHOR INFORMATION

Corresponding Authors

R. Scott Smith − *Physical Sciences Division, Pacific Northwest National Laboratory, Richland, Washington 99352, United States*; orcid.org/0000-0002-7145-1963; Email: Scott.Smith@pnnl.gov

Bruce D. Kay − *Physical Sciences Division, Pacific Northwest National Laboratory, Richland, Washington 99352, United States*; orcid.org/0000-0002-8543-2341; Email: Bruce.Kay@pnnl.gov

Authors

Wyatt A. Thornley − *Physical Sciences Division, Pacific Northwest National Laboratory, Richland, Washington 99352, United States*

Greg A. Kimmel − *Physical Sciences Division, Pacific Northwest National Laboratory, Richland, Washington 99352, United States*; orcid.org/0000-0003-4447-2440

Complete contact information is available at: https://pubs.acs.org/10.1021/acs.jpclett.5c00245

Notes

The authors declare no competing financial interest.

■ ACKNOWLEDGMENTS

This work was supported by the U.S. Department of Energy (DOE), Office of Science, Office of Basic Energy Sciences, Division of Chemical Sciences, Geosciences, and Biosciences (FWP 16248).

■ REFERENCES

(1) Debenedetti, P. G. Supercooled and Glassy Water. *J. Phys.: Condens. Matter* **2003**, *15*, R1669.

(2) Angell, C. A. Insights into Phases of Liquid Water from Study of Its Unusual Glass-Forming Properties. *Science* **2008**, *319*, 582−587.

(3) Gallo, P.; Arnann-Winkel, K.; Angell, C. A.; Anisimov, M. A.; Caupin, F.; Chakravarty, C.; Lascaris, E.; Loerting, T.; Panagiotopoulos, A. Z.; Russo, J.; Sellberg, J. A.; Stanley, H. E.; Tanaka, H.; Vega, C.; Xu, L. M.; Pettersson, L. G. M. Water: A Tale of Two Liquids. *Chem. Rev.* **2016**, *116*, 7463−7500.

(4) Amann-Winkel, K.; Bohmer, R.; Fujara, F.; Gainaru, C.; Geil, B.; Loerting, T. Colloquium: Water's Controversial Glass Transitions. *Rev. Mod. Phys.* **2016**, *88*, 011002.

(5) Speedy, R. J.; Angell, C. A. Isothermal Compressibility of Supercooled Water and Evidence for a Thermodynamic Singularity at −45degreesc. *J. Chem. Phys.* **1976**, *65*, 851−858.

(6) Prielmeier, F. X.; Lang, E. W.; Speedy, R. J.; Ludemann, H. D. Diffusion in Supercooled Water to 300-Mpa. *Phys. Rev. Lett.* **1987**, *59*, 1128−1131.

(7) Speedy, R. J. Evidence for a New Phase of Water - Water-II. *J. Phys. Chem.* **1992**, *96*, 2322−2325.

(8) Johari, G. P.; Fleissner, G.; Hallbrucker, A.; Mayer, E. Thermodynamic Continuity between Glassy and Normal Water. *J. Phys. Chem.* **1994**, *98*, 4719−4725.

(9) Speedy, R. J.; Debenedetti, P. G.; Smith, R. S.; Huang, C.; Kay, B. D. The Evaporation Rate, Free Energy, and Entropy of Amorphous Water at 150 K. *J. Chem. Phys.* **1996**, *105*, 240−244.

(10) Debenedetti, P. G.; Stillinger, F. H. Supercooled Liquids and the Glass Transition. *Nature* **2001**, *410*, 259−267.

(11) Ediger, M. D.; Angell, C. A.; Nagel, S. R. Supercooled Liquids and Glasses. *J. Phys. Chem.* **1996**, *100*, 13200−13212.

(12) Debenedetti, P. G. *Metastable Liquids: Concepts and Principles*; Princeton University Press: 1996; Vol. *1*.

(13) Angell, C. A. Amorphous Water. *Annu. Rev. Phys. Chem.* **2004**, *55*, 559−583.

(14) Debenedetti, P. G.; Stanley, H. E. Supercooled and Glassy Water. *Phys. Today* **2003**, *56*, 40−46.

(15) Smith, R. S.; Kay, B. D. The Existence of Supercooled Liquid Water at 150 K. *Nature* **1999**, *398*, 788−791.

(16) Smith, R. S.; Petrik, N. G.; Kimmel, G. A.; Kay, B. D. Thermal and Nonthermal Physiochemical Processes in Nanoscale Films of Amorphous Solid Water. *Acc. Chem. Res.* **2012**, *45*, 33−42.

(17) Johari, G. P.; Hallbrucker, A.; Mayer, E. The Glass Liquid Transition of Hyperquenched Water. *Nature* **1987**, *330*, 552−553.

(18) Hallbrucker, A.; Mayer, E.; Johari, G. P. Glass-Liquid Transition and the Enthalpy of Devitrification of Annealed Vapor-Deposited Amorphous Solid Water - a Comparison with Hyper-quenched Glassy Water. *J. Phys. Chem.* **1989**, *93*, 4986−4990.

(19) Johari, G. P. Liquid State of Low-Density Pressure-Amorphized Ice above Its T-G. *J. Phys. Chem. B* **1998**, *102*, 4711−4714.

(20) Kohl, I.; Bachmann, L.; Mayer, E.; Hallbrucker, A.; Loerting, T. Water Behaviour - Glass Transition in Hyperquenched Water? *Nature* **2005**, *435*, No. E1.

(21) Ito, K.; Moynihan, C. T.; Angell, C. A. Thermodynamic Determination of Fragility in Liquids and a Fragile-to-Strong Liquid Transition in Water. *Nature* **1999**, *398*, 492−495.

(22) Yue, Y. Z.; Angell, C. A. Clarifying the Glass-Transition Behaviour of Water by Comparison with Hyperquenched Inorganic Glasses. *Nature* **2004**, *427*, 717−720.

(23) Fisher, M.; Devlin, J. P. Defect Activity in Amorphous Ice from Isotopic Exchange Data - Insight into the Glass-Transition. *J. Phys. Chem.* **1995**, *99*, 11584−11590.

(24) Shephard, J. J.; Salzmann, C. G. Molecular Reorientation Dynamics Govern the Glass Transitions of the Amorphous Ices. *J. Phys. Chem. Lett.* **2016**, *7*, 2281−2285.

(25) Smith, R. S.; Huang, C.; Kay, B. D. Evidence for Molecular Translational Diffusion during the Crystallization of Amorphous Solid Water. *J. Phys. Chem. B* **1997**, *101*, 6123−6126.

(26) Smith, R. S.; Dohnalek, Z.; Kimmel, G. A.; Stevenson, K. P.; Kay, B. D. The Self-Diffusivity of Amorphous Solid Water near 150 K. *Chem. Phys.* **2000**, *258*, 291−305.

(27) McClure, S. M.; Barlow, E. T.; Akin, M. C.; Safarik, D. J.; Truskett, T. M.; Mullins, C. B. Transport in Amorphous Solid Water Films: Implications for Self-Diffusivity. *J. Phys. Chem. B* **2006**, *110*, 17987−17997.

(28) McClure, S. M.; Safarik, D. J.; Truskett, T. M.; Mullins, C. B. Evidence That Amorphous Water Below 160 K Is Not a Fragile Liquid. *J. Phys. Chem. B* **2006**, *110*, 11033−11036.

(29) Smith, R. S.; Matthiesen, J.; Knox, J.; Kay, B. D. Crystallization Kinetics and Excess Free Energy of H_2O and D_2O Nanoscale Films of Amorphous Solid Water. *J. Phys. Chem. A* **2011**, *115*, 5908−5917.

(30) Murphy, D. M.; Koop, T. Review of the Vapour Pressures of Ice and Supercooled Water for Atmospheric Applications. *Quarterly Journal of the Royal Meteorological Society* **2005**, *131*, 1539−1565.

(31) Smith, R. S.; Huang, C.; Wong, E. K. L.; Kay, B. D. The Molecular Volcano: Abrupt CCl_4 Desorption Driven by the Crystallization of Amorphous Solid Water. *Phys. Rev. Lett.* **1997**, *79*, 909−912.

(32) May, R. A.; Smith, R. S.; Kay, B. D. The Molecular Volcano Revisited: Determination of Crack Propagation and Distribution during the Crystallization of Nanoscale Amorphous Solid Water Films. *J. Phys. Chem. Lett.* **2012**, *3*, 327−331.

(33) May, R. A.; Smith, R. S.; Kay, B. D. The Release of Trapped Gases from Amorphous Solid Water Films. II. ″Bottom-up″ Induced Desorption Pathways. *J. Chem. Phys.* **2013**, *138*, 104502.

(34) May, R. A.; Smith, R. S.; Kay, B. D. The Release of Trapped Gases from Amorphous Solid Water Films. I. ″Top-down″ Crystallization-Induced Crack Propagation Probed Using the Molecular Volcano. *J. Chem. Phys.* **2013**, *138*, 104501.

(35) Jakli, G.; Staschewski, D. Vapour Pressure of H218o Ice (−50 to 0°C) and H218o Water (0 to 170°C). *Journal of the Chemical Society, Faraday Transactions 1: Physical Chemistry in Condensed Phases* **1977**, *73*, 1505−1509.

(36) Kudish, A. I.; Wolf, D.; Steckel, F. Physical Properties of Heavy-Oxygen Water. Absolute Viscosity of H218o between 15 and 35°C. *Journal of the Chemical Society, Faraday Transactions 1: Physical Chemistry in Condensed Phases* **1972**, *68*, 2041−2046.

(37) Xu, Y.; Petrik, N. G.; Smith, R. S.; Kay, B. D.; Kimmel, G. A. Growth Rate of Crystalline Ice and the Diffusivity of Supercooled Water from 126 to 262 K. *Proceedings of the National Academy of Science USA* **2016**, *113*, 14921−14925.

(38) Yuan, C. Q.; Smith, R. S.; Kay, B. D. Communication: Distinguishing between Bulk and Interface-Enhanced Crystallization in Nanoscale Films of Amorphous Solid Water. *J. Chem. Phys.* **2017**, *146*, 031102.

(39) Smith, R. S.; Yuan, C. Q.; Petrik, N. G.; Kimmel, G. A.; Kay, B. D. Crystallization Growth Rates and Front Propagation in Amorphous Solid Water Films. *J. Chem. Phys.* **2019**, *150*, 214703.

(40) Cahn, J. W.; Hillig, W. B.; Sears, G. W. Molecular Mechanism of Solidification. *Acta Metall.* **1964**, *12*, 1421.

(41) Jackson, K. A.; Uhlmann, D. R.; Hunt, J. D. On the Nature of Crystal Growth from the Melt. *J. Cryst. Growth* **1967**, *1*, 36.

(42) Broughton, J. Q.; Gilmer, G. H.; Jackson, K. A. Crystallization Rates of a Lennard-Jones Liquid. *Phys. Rev. Lett.* **1982**, *49*, 1496−1500.

(43) Ngai, K. L.; Magill, J. H.; Plazek, D. J. Flow, Diffusion and Crystallization of Supercooled Liquids: Revisited. *J. Chem. Phys.* **2000**, *112*, 1887−1892.

(44) Jackson, K. A. *Kinetic Processes: Crystal Growth, Diffusion, and Phase Transitions in Materials*; Wiley-VCH: 2004.

(45) Mapes, M. K.; Swallen, S. F.; Ediger, M. D. Self-Diffusion of Supercooled O-Terphenyl near the Glass Transition Temperature. *J. Phys. Chem. B* **2006**, *110*, 507−511.

(46) Matthiesen, J.; Smith, R. S.; Kay, B. D. Using Rare Gas Permeation to Probe Methanol Diffusion near the Glass Transition Temperature. *Phys. Rev. Lett.* **2009**, *103*, 245902.

(47) Matthiesen, J.; Smith, R. S.; Kay, B. D. Measuring Diffusivity in Supercooled Liquid Nanoscale Films Using Inert Gas Permeation. II. Diffusion of Ar, Kr, Xe, and CH_4 through Methanol. *J. Chem. Phys.* **2010**, *133*, 174505.

(48) Smith, R. S.; Matthiesen, J.; Kay, B. D. Breaking through the Glass Ceiling: The Correlation between the Self-Diffusivity in and Krypton Permeation through Deeply Supercooled Liquid Nanoscale Methanol Films. *J. Chem. Phys.* **2010**, *132*, 124502.

(49) Smith, R. S.; Matthiesen, J.; Kay, B. D. Measuring Diffusivity in Supercooled Liquid Nanoscale Films Using Inert Gas Permeation. I. Kinetic Model and Scaling Methods. *J. Chem. Phys.* **2010**, *133*, 174504.

(50) Matthiesen, J.; Smith, R. S.; Kay, B. D. Probing the Mobility of Supercooled Liquid 3-Methylpentane at Temperatures near the Glass Transition Using Rare Gas Permeation. *J. Chem. Phys.* **2012**, *137*, 064509.

(51) Swallen, S. F.; Kearns, K. L.; Mapes, M. K.; Kim, Y. S.; McMahon, R. J.; Ediger, M. D.; Wu, T.; Yu, L.; Satija, S. Organic Glasses with Exceptional Thermodynamic and Kinetic Stability. *Science* **2007**, *315*, 353−356.

(52) Zhang, Y.; Glor, E. C.; Li, M.; Liu, T. Y.; Wahid, K.; Zhang, W.; Riggleman, R. A.; Fakhraai, Z. Long-Range Correlated Dynamics in Ultra-Thin Molecular Glass Films. *J. Chem. Phys.* **2016**, *145*, 114502.

(53) Zhang, Y.; Fakhraai, Z. Decoupling of Surface Diffusion and Relaxation Dynamics of Molecular Glasses. *Proc. Natl. Acad. Sci. U.S.A.* **2017**, *114*, 4915−4919.

(54) Cheng, L.; Fenter, P.; Nagy, K. L.; Schlegel, M. L.; Sturchio, N. C. Molecular-Scale Density Oscillations in Water Adjacent to a Mica Surface. *Phys. Rev. Lett.* **2001**, *87*, 156103.

(55) Cicero, G.; Grossman, J. C.; Schwegler, E.; Gygi, F.; Galli, G. Water Confined in Nanotubes and between Graphene Sheets: A First Principle Study. *J. Am. Chem. Soc.* **2008**, *130*, 1871−1878.

(56) Limmer, D. T.; Willard, A. P.; Madden, P.; Chandler, D. Hydration of Metal Surfaces Can Be Dynamically Heterogeneous and Hydrophobic. *Proc. Natl. Acad. Sci. U.S.A.* **2013**, *110*, 4200−4205.

(57) Bourg, I. C.; Steefel, C. I. Molecular Dynamics Simulations of Water Structure and Diffusion in Silica Nanopores. *J. Phys. Chem. C* **2012**, *116*, 11556−11564.

(58) Gasparotto, P.; Fitzner, M.; Cox, S. J.; Sosso, G. C.; Michaelides, A. How Do Interfaces Alter the Dynamics of Supercooled Water? *Nanoscale* **2022**, *14*, 4254−4262.

(59) Chen, S. H.; Liao, C.; Sciortino, F.; Gallo, P.; Tartaglia, P. Model for Single-Particle Dynamics in Supercooled Water. *Phys. Rev. E* **1999**, *59*, 6708−6714.

(60) Brovchenko, I.; Paschek, D.; Geiger, A. Gibbs Ensemble Simulation of Water in Spherical Cavities. *J. Chem. Phys.* **2000**, *113*, 5026−5036.

(61) Takahara, S.; Sumiyama, N.; Kittaka, S.; Yamaguchi, T.; Bellissent-Funel, M. C. Neutron Scattering Study on Dynamics of Water Molecules in Mcm-41. 2. Determination of Translational Diffusion Coefficient. *J. Phys. Chem. B* **2005**, *109*, 11231−11239.

(62) Briman, I. M.; Rébiscoul, D.; Diat, O.; Zanotti, J. M.; Jollivet, P.; Barboux, P.; Gin, S. Impact of Pore Size and Pore Surface Composition on the Dynamics of Confined Water in Highly Ordered Porous Silica. *J. Phys. Chem. C* **2012**, *116*, 7021−7028.

(63) Oguni, M.; Angell, C. A. Heat-Capacities of H_2O+H_2O_2, and H_2O+N_2H_4, Binary-Solutions - Isolation of a Singular Component for Cp of Supercooled Water. *J. Chem. Phys.* **1980**, *73*, 1948−1954.

(64) Kringle, L.; Thornley, W. A.; Kay, B. D.; Kimmel, G. A. Reversible Structural Transformations in Supercooled Liquid Water from 135 to 245 K. *Science* **2020**, *369*, 1490.

(65) Kringle, L.; Kay, B. D.; Kimmel, G. A. Structural Relaxation of Water during Rapid Cooling from Ambient Temperatures. *J. Chem. Phys.* **2023**, *159*, 064509.

(66) Krueger, C. R.; Mowry, N. J.; Bongiovanni, G.; Drabbels, M.; Lorenz, U. J. Electron Diffraction of Deeply Supercooled Water in No Man's Land. *Nat. Commun.* **2023**, *14*, 2812.

(67) Smith, R. S.; Zubkov, T.; Kay, B. D. The Effect of the Incident Collision Energy on the Phase and Crystallization Kinetics of Vapor Deposited Water Films. *J. Chem. Phys.* **2006**, *124*, 114710.

(68) Kimmel, G. A.; Stevenson, K. P.; Dohnalek, Z.; Smith, R. S.; Kay, B. D. Control of Amorphous Solid Water Morphology Using Molecular Beams. I. Experimental Results. *J. Chem. Phys.* **2001**, *114*, 5284.

(69) Stevenson, K. P.; Kimmel, G. A.; Dohnalek, Z.; Smith, R. S.; Kay, B. D. Controlling the Morphology of Amorphous Solid Water. *Science* **1999**, *283*, 1505.

(70) Kimmel, G. A.; Petrik, N. G.; Dohnalek, Z.; Kay, B. D. Crystalline Ice Growth on Pt(111): Observation of a Hydrophobic Water Monolayer. *Phys. Rev. Lett.* **2005**, *95*, 166102.

(71) Kimmel, G. A.; Petrik, N. G.; Dohnálek, Z.; Kay, B. D. Crystalline Ice Growth on Pt(111) and Pd(111):: Nonwetting Growth on a Hydrophobic Water Monolayer. *J. Chem. Phys.* **2007**, *126*, 114702.